3D shape reconstruction of optical element using polarization

M. Vedel[a], N. Lechocinski[a], S. Breugnot[a]
[a]Bossa Nova Technologies, 606 Venice Blvd, Suite B, Venice, CA90291, USA

ABSTRACT

We present a novel polarization based metrological method of 3D shape measurement for in-line control of optical surfaces and control of highly aspheric optical surfaces. This technique is fast, non contact, high resolution, alignment free and with unprecedented dynamic. It has the potential to reach tens of nanometers accuracy. In this paper we show that a polarization imaging camera combined with an un-polarized illumination and 3D reconstruction algorithm lead to the 3D reconstruction of optical element (regular lens and aspheric lens) and the measurement of their parameters. The optical element to be measured is placed in a diffusive integrating sphere and illuminated by un-polarized light. The reflection of the un-polarized light by the optical element gets partially polarized. A polarization camera captures the image of the optical element and measures the polarization state of each pixel in real time. The Degree Of Light Polarized and the Angle Of Polarization parameters are related to the geometry of the optical element. The 3D shape of the optical element is reconstructed using dedicated software. The architecture of the hardware, calibration results and sensitivity measurements is presented and experimental results and observations as well as possible further steps and new applications are discussed.

Keywords: 3D reconstruction, polarization imaging, linear Stokes parameters, metrology

1. INTRODUCTION

In this paper, we describe the results of a feasibility study for the development of a polarization based metrological method of 3D shape measurement for in-line control of optical surfaces and control of highly aspheric optical surfaces. The method uses the "Shape from Polarization" method developed by Miyazaki [1-3], Rahman [4-6] and Atkinson [7-9] among others for the reconstruction of dielectric surfaces. This technique is based on the polarization imaging of the optical element, leading to the measurement of the polarization state for each pixel of the image. This allows the reconstruction of the 3D shape of the imaged optical element.

With increasing requirement for improving productivity and competitiveness, manufacturing companies are looking to implement more in-line inspection techniques where the immediate feedback can lead to tighter tolerance, reduction in scraps and reduction in energy consumption. In this paper, we show that a fast polarization imaging camera combined with an un-polarized illumination and a 3D reconstruction algorithm led to the 3D reconstruction of optical element (regular lens and aspheric lens) and the measurement of their parameters.

The current measurement methods (interferometers, contact profilometers) of optical surfaces are not adapted to high volume as they are either fast but require precise alignment (optical methods) or not sensitive to alignment but very slow (mechanical methods). Tomorrow's optical surfaces will be very aspheric and have high numerical aperture to meet the requirements of smaller and more cost effective optics. The current optical production is currently shifting toward these lenses which are difficult or too slow to control with current methods. Using a fast polarization camera [16] instead of a rotating mechanical polarizer allows performing the 3D reconstruction in less than 30 seconds.

In the developed polarization method of 3D shape measurement, the optical element to be measured is placed in a diffusive integrating sphere and illuminated by un-polarized light. The reflection of the un-polarized light by the optical element gets partially polarized according to Fresnel's laws [12,13]. A polarization camera captures the image of the optical element and measures the polarization state of each pixel in real time. The polarization state being related to the geometry of the optical element, the 3D shape of the optical element can be reconstructed using dedicated software.

This paper starts with a theoretical paragraph to remind the principle of the method and the main tasks to be carried out. Then the developed setup, software and the several tests performed to evaluate their performances are described. Finally we discuss these results and the further steps to be addressed.

2. 3D RECONSTRUCTION BASED ON POLARIZATION IMAGING

2.1 Description of polarization

Light can be totally polarized, unpolarized or partially polarized. A totally polarized light can then be linearly polarized, circularly polarized, or elliptically polarized. An unpolarized light is a light which has no coherence between the electric fields along to orthogonal directions. In between light can be partially polarized. The polarization state of light is usually described using Stokes formalism (Equation 1) [13].

$$\vec{S} = \begin{bmatrix} S_0 \\ S_1 \\ S_2 \\ S_3 \end{bmatrix} \qquad \begin{aligned} S_0 &= \left\langle E_x E_x^* + E_y E_y^* \right\rangle = I_{0^\circ} + I_{90^\circ} \\ S_1 &= \left\langle E_x E_x^* - E_y E_y^* \right\rangle = I_{0^\circ} - I_{90^\circ} \\ S_2 &= \left\langle E_x E_y^* + E_y E_x^* \right\rangle = I_{45^\circ} - I_{-45^\circ} \\ S_3 &= j\left\langle E_x E_y^* - E_y E_x^* \right\rangle = I_{lh} - I_{rh} \end{aligned} \tag{1}$$

It can describe any type of polarization and is linear with the intensity of light which makes it compatible with linear algebra. The Stokes-Mueller formalism describes mathematically the polarization of light as well as its evolution. This formalism uses real quadratic values (intensities along horizontal, vertical axes...) directly measured by detectors. A Stokes vector is a 4 components vector. However, polarization is generally described with more physical parameters. The parameters relevant for this paper are the Degree Of Linear Polarization (DOLP) and Angle Of linear Polarization (AOP) (Equation 2). DOLP represents the relative amount of light linearly polarized; AOP represents the orientation of this linearly polarized part.

$$\begin{aligned} DOLP &= \left\| \frac{S_1 + iS_2}{S_0} \right\| \\ AOP &= \frac{1}{2} Arg\left(S_1 + iS_2\right) \end{aligned} \tag{2}$$

2.2 Fresnel equations

Generally speaking, polarization of light will be modified after interacting with an object [12,13]. The possible modifications include, but are not limited to, depolarization of a polarized light and polarization of an unpolarized light. Polarization of an unpolarized light is a very general phenomenon. It comes from a difference in the reflection coefficient for the electric field in the plane of incidence and perpendicular to the plane of incidence. This difference in the reflection coefficient is perfectly determined by the angle of incidence on the surface and the physical properties of the material. The reflection coefficient for the electric field in the plane of incidence (p-polarization) and perpendicular to the plane of incidence (s-polarization) are calculated using the Fresnel equations [12]. The fact that the reflection coefficients are not the same makes that an unpolarized light will become partially s-polarized after a reflection by a dielectric surface (figure 1). Using the Fresnel equations, the DOLP can be calculated for any angle of incidence $\boldsymbol{\theta}$ (Equation 3). The calculation of the DOLP after a specular reflection of light by a dielectric surface shows that a measurement of DOLP can be inverted to two possible angles of incidence with the hypothesis of a known material refractive index and unpolarized incident light [1-11]. The same calculation can be conducted for other surfaces materials. Morel described an extension of the “Shape from Polarization” method to metallic surfaces using a complex refractive index [10,11].

$$DOLP_{reflection} = \frac{2\sin^2\theta\sqrt{n^2 - \sin^2\theta - n^2\sin^2\theta - \sin^4\theta}}{n^2 - \sin^2\theta - n^2\sin^2\theta - 2\sin^4\theta} \quad (3)$$

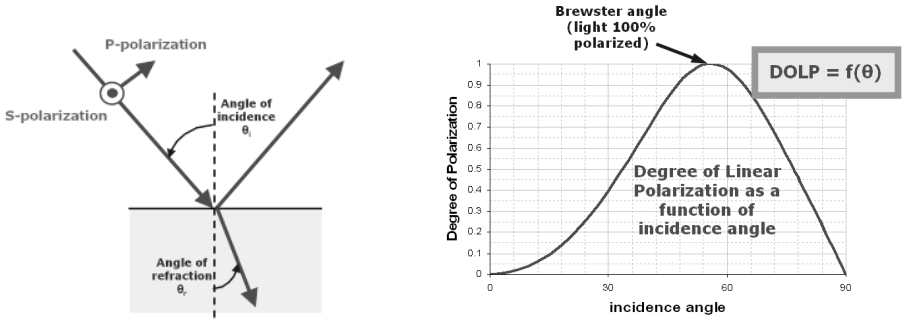

Figure 1. Fresnel laws: light reflected by a dielectric surface becomes partially polarized depending on the incidence angle

2.3 Shape from polarization

Gradient field estimation

Given a conventional Cartesian coordinate system (X,Y,Z) one can express the 3D shape by the height Z in function of (X,Y) parameters. The method presented in this paper is based on the surface gradient field reconstruction and its numerical integration. Figure 2 shows the geometrical parameters. Each normal vector (Equation 3) is expressed knowing the local slope, related to the zenith angle θ_i (incidence angle of the light), and the azimuth angle φ [1-11].

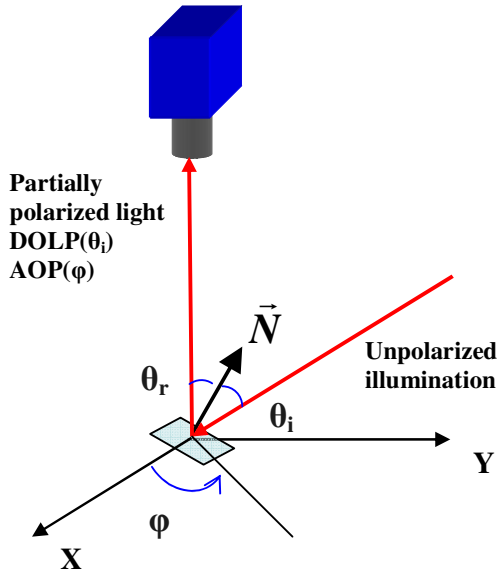

$$\vec{N} = \begin{pmatrix} p = \tan(\theta)\cos(\varphi) \\ q = \tan(\theta)\sin(\varphi) \\ 1 \end{pmatrix} = \begin{pmatrix} -\frac{\partial Z(X,Y)}{\partial X} \\ -\frac{\partial Z(X,Y)}{\partial Y} \\ 1 \end{pmatrix} \quad (3)$$

Figure 2. Geometrical parameters

Considering a specular reflection on the surface element the incidence angle θ_i and the reflected angle θ_r are the same. We will denote it the zenith angle θ. The Fresnel equations link the surface's local slope (zenith angle), the refractive index **n** of the material and the Degree Of Linear Polarization (Equation 3). This equation can be inverted to express the two zenith angles θ possible: one below and one above the Brewster incidence angle (figure 1). In most of the cases, the first root will be the right one. For a usual glass with refractive index around 1.5, Brewster's angle is 56°. Most of the optics do not have such high slope. Even high numerical apertures aspherics or condensers have slopes below 45° at their edge. The results presented in this paper are limited to these cases.

The second parameter φ is related to the Angle Of Polarization. As the polarization vector is defined within [0°; 180°] cycle there are two possible azimuth angles for the normal vector (Equation 4).

$$\varphi = AOP \quad \text{or} \quad \varphi = AOP + \pi \tag{4}$$

Several methods to resolve that ambiguity have been described in previous papers [1-11]. A simple algorithm has been used to disambiguate the normal to the surface. As shown in figure 3, for simple lenses shape, the normal to the surface appear to radiate for the point of the lens oriented toward the lens. The angle θ also increases with the radius. These are the properties used to disambiguate the normal to the surface for simple shape lenses: convex or concave surfaces with no inflexion point.

Gradient field integration

Once the zenith and the azimuth angles are known for each pixel of the imaged sample we need to operate a numerical integration in order to obtain the 3D height map Z(X,Y). Many off the shelf algorithms to project a gradient field onto the closest integrable gradient field and to recover the 3D surface associated with this gradient field exist. The most used is the Frankot-Chellapa algorithm [14]. The non integrable gradient field measured is projected onto a base of integrable functions which are the Fourier functions. Let us denote $\tilde{Z}$, $\tilde{p}$ and $\tilde{q}$ the Fourier transform of respectively the height map and the X, Y components of the gradient field; μ and ν the reciprocal coordinates in the Fourier space. Then the Fourier transform of the height map can be expressed as Equation (4) for each pixel.

$$\tilde{Z}(\mu,\nu) = \frac{-i.\mu.\tilde{p}^* - i.\nu.\tilde{q}^*}{\mu^2 + \nu^2} \tag{4}$$

Finally an inverse Fourier transform operation is computed in order to obtain the height map of the sample's surface. This algorithm is very efficient in term of both precision of the results and speed.

3. EXPERIMENTAL SETUP

3.1 Illumination design

As we measure the amount of polarized light reflected by the sample to be characterized, an unpolarized illumination had to be designed. It is based on an integrating sphere which uses a white Lambertian coating. The light source used is made of 2 green LEDs. These LEDs were chosen for several reasons: first of all, they provide high luminous flux, typically 160 lm per LED. They have a narrow spectrum, which is an advantage as the polarization elements used in the polarization camera presents some chromatic dependency of its polarization properties. Figure 3 shows pictures of the sphere.

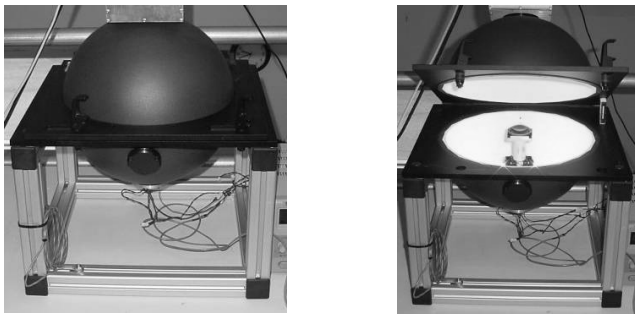

Figure 3. Picture of the integrating sphere (a) Closed (b) Open with illumination

3.2 Polarization camera

The polarization camera used is composed of a fast polarization modulator developed by Bossa Nova Technologies [16]. It allows switching polarization state between 4 linear polarization states (0°, 45°, 90° and 135°). The camera is able to perform polarization imaging of a scene. With the 4 polarization images acquired in real time, it is easy to calculate the linear Stokes parameters and the following polarization parameters - Degree of Linear Polarization (DOLP) and the Angle of Polarization (AOP) – for each pixel of the image. The polarization camera is based on a standard CCD camera. This CCD camera has good capacity, resolution, noise and linearity. Figure 4 shows the polarization camera mounted vertically to image the sample that is mounted inside the integrating sphere.

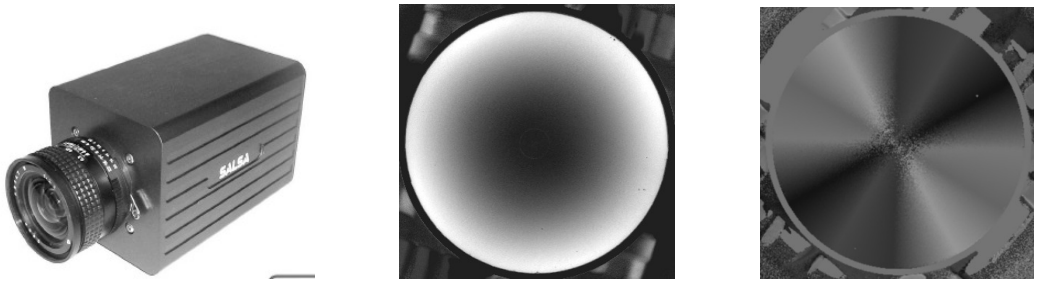

Figure 4. (a) Bossa Nova Technologies linear Stokes camera SALSA^{TM} (b) DOLP grayscale image of a 1'' aspheric lens (c) AOP as a color HUE

The DOLP is increasing with the radius, as the slope of the optic is; the AOP is varying according to the azimuth angle.

3.3 Sample mount

The measurement is based on the analysis of the light reflected by the first surface of the sample. To be able to measure only the light reflected by the first surface**,** it is necessary to remove any other reflected and scattered light coming from the back surface of the sample or from the holder. The sample needs to be both opaque and non scattering. This can be achieved by index matching the back surface of lens to the support. In this case, the support must have the same refractive index as the lens. The best to this end is to use an absorptive glass optical density and index matching liquid (figure 5).

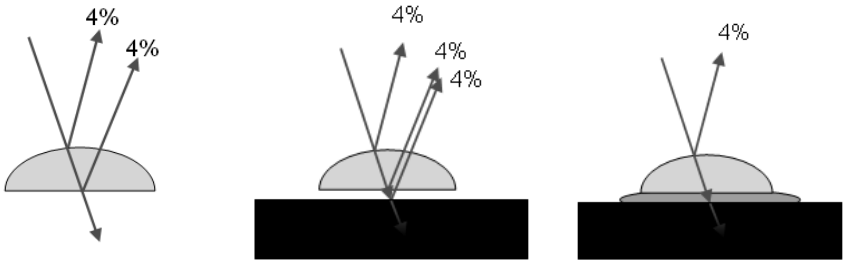

Figure 5: (a) the specular reflection at an air-glass interface is characterized by a 4% reflection coefficient. (b) Using an optical density as a support avoids both transmitted and scattered light. (c) Index matching the optical density and the lens eliminates the surface reflections

We used an index matching liquid of refractive index n=1.52. The refractive index of BK7 (most commonly used glass) is exactly this value around 520nm (green). To test the efficiency of the set up, we imaged the lens on the absorptive neutral density without index matching liquid, with water (refractive index 1.33) as index matching material and finally with the index matching material (figure 6). Without index matching material, a strong back reflection is visible. It is even brighter than the front reflection because it comes from the interface between the lens and air and from the interface between the absorptive neutral density and air. Interferences fringes are visible on the back surface reflection (equal thickness interference fringes). The reflections at the back surface are about to 8% of the total light which is twice as much as the front surface reflection. With water as index matching material, the back surface reflections are highly attenuated but are still not negligible in front on the front surface reflection. The total reflection coefficient is about 0.9%. With the index matching liquid, the back reflection totally disappears; only the front surface reflection is visible.

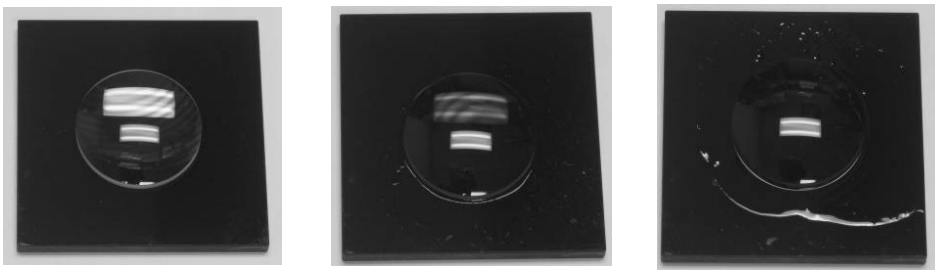

Figure 6: (a) lens on an absorptive optical density. The back surface reflection is stronger than front surface reflection. (b) Using water as index matching material dramatically reduces back surface reflection. (c) Using a specific index matching liquid totally eliminates the back surface reflection

3.4 Full Setup

Figure 7 shows a picture of the complete system, showing the polarization camera, the integrating sphere and the sample.

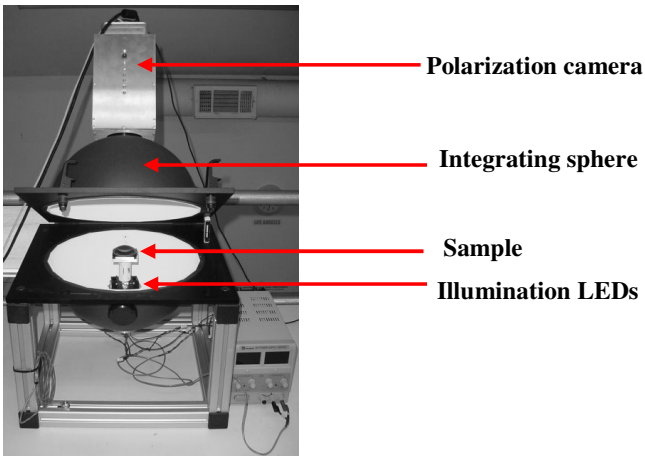

Figure 7. Full Setup

4. TESTS ON COMMERCIAL SAMPLES - ANALYSIS

In order to evaluate the performances and the limitations of the developed system we realized many tests on several spherical and aspheric commercial samples. Measurements were performed on spherical lenses with Radius of Curvature ranging from 15mm to 110mm. Profiles can be deduced from the 3D shape and compared to theoretical values. The repeatability of the measurement can be evaluated by subtracting two measurements. Figure 8 shows a screenshot of a sample's surface 3D reconstruction (a), the selection of a section profile to be plotted (b) and an extracted profile (c).

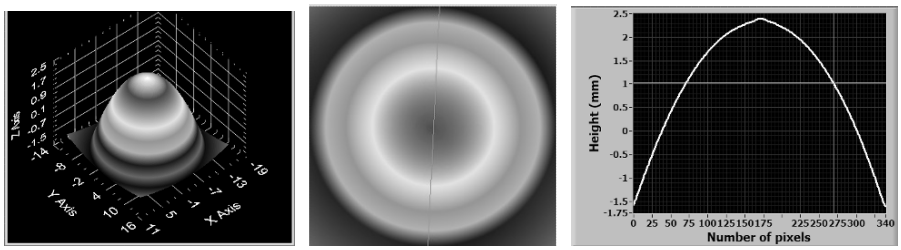

Figure 8. (a)Reconstructed surface, (b) section (c) extracted profile

4.1 Tests on commercial samples

Profile measurements

Profile measurements were performed on commercial highly aspheric lenses. These profiles were compared to very accurate measured profiles (performed with 250nm resolution mechanical profilometer) given by the constructor in order to evaluate the performances of the system. Figure 9 shows a profile measured on a commercial aspheric lens sample with a high departure from sphere parameter (conic constant: k = -2.27, Departure From Sphere=180µm). The red curve shows the profile acquired by the constructor's contact profilometer (1nm resolution) and the black curve shows the one acquired by our system.

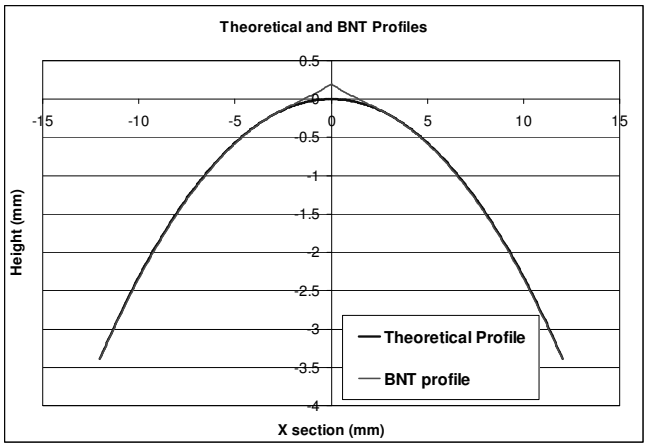

Figure 9: Measured and theoretical profiles – aspheric sample

One can notice the strong artifact at the top of the surface. It is due to the reflection of the diaphragm on the sample surface which modifies the DOLP value. The DOLP is already very low on the central area of the sample because the incident angle of the light beam is very close to the normal direction. So the combination of those two parameters leads to that strong artifact. Figure 10 shows the plot of the difference between the reconstructed and the theoretical profile. If we forget the strong artifact at the center due to the reflection of the pupil lens on the sample we can notice that the error is a slowly increasing in the field and has a rotational symmetry component. The maximum amplitude is around 25µm at the edge of the sample. There is a strong field dependency. However, we think that dependency is an artifact and does not show the real limitation of the reconstruction method. The real limitation is more likely to be the high frequency noise around the slow variation. The amplitude of that noise is about 100nm which correspond to the order of magnitude given by our previous simulations. In the following section we will analyze the possible sources of these artifacts.

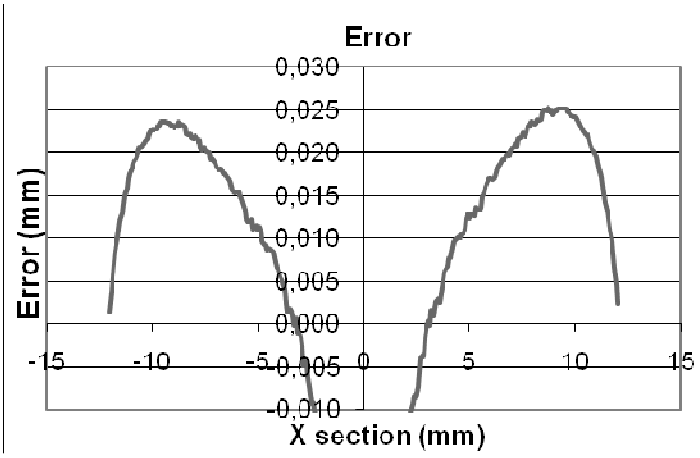

Figure 10. Difference between the theoretical and the reconstructed profile

Repeatability

Several measurements in a row were performed on the same sample (removing the sample from the holder) in order to evaluate the repeatability of the results. Reconstructed surfaces of two successive acquisitions are subtracted. Residual noise and artifacts can be estimated. Figure 11 shows the 3D residual noise of two measurements on a 20.6mm ROC sample (sample removed between the 2 measurements). The PV value of the residual surface is 1.9µm. This is extremely encouraging as the measurements are done without any specific optical alignment like the ones required for interferometric methods.

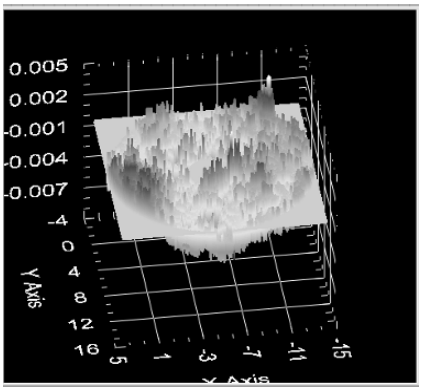

Figure 11. Measurement repeatability

5. CURRENT LIMITATIONS – FURTHER STEPS

These preliminary tests were very useful to estimate the limitations of the system. The main limitations are the artifact due to the central reflection and the slow deviation observed which is increasing with the field of view. The potential sources of errors investigated are listed below:

- Artifacts in the 3D reconstruction algorithm itself
- The measurement of DOLP and AOP parameters

5.1 Artifacts introduced by the algorithm

The point is to evaluate the error introduced by the reconstruction algorithm itself. We generated perfect DOLP and AOP map and used the reconstruction algorithm. Then we can compare the reconstructed spheres with a theoretical sphere and see the defects introduced by the algorithm. Then we have computed the difference between the reconstructed shape and the theoretical one. Figure 12 shows the 3D plot and an extracted profile of that difference

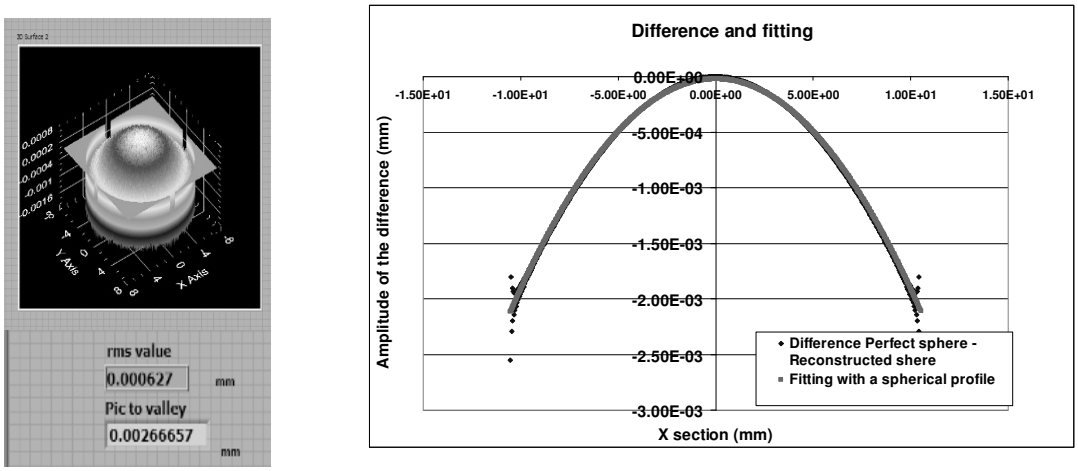

Figure 12: 3D plot (a) and profile (b) of the deviation between perfect sphere and reconstructed sphere

The PV amplitude of the deviation is around 2.7µm for a simulated 40 mm Radius Of Curvature. Moreover the profile shape of the deviation appears to be spherical and using a numerical solver we can estimate the best sphere parameters which fit the deviation profile (especially the Radius Of Curvature of the deviation profile). Figure 13 shows that the ROC of the deviation profile is proportional to the ROC of the sphere to be reconstructed.

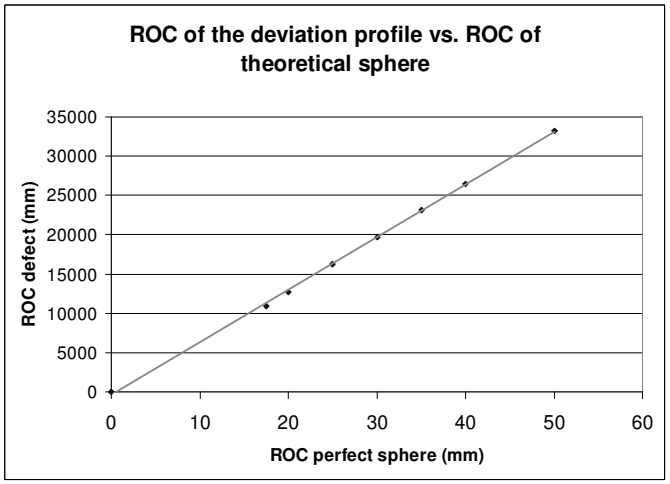

Figure 13: ROC of the profile deviation vs. ROC of the sphere

These tests have shown that the algorithm itself introduces artifact in the 3D reconstructed shape. Those artifacts strongly depend on the geometric parameters of the system. The PV amplitude of the defect ranges from 2 to 4µm depending on the Radius Of Curvature of the sphere and on geometrical parameters. The reconstruction process assumes that the distance between the entrance pupil and the sample as well as the magnification of the optical conjugation is uniform. In reality, as shown in figure 14, these parameters vary in the field. This is particularly true with high sag optics such as the tested aspherics. That explains why the ROC of the deviation profile is increasing with the ROC of the sphere to be reconstructed. The more the ROC of the sphere is, the less the sag is, and the less the amplitude of the deviation is. The consequences are a non uniform integration of the gradient field and could lead to such an artifact. The same kind of error has been observed in the measurement of the DOLP parameter; it will be detailed in the following section.

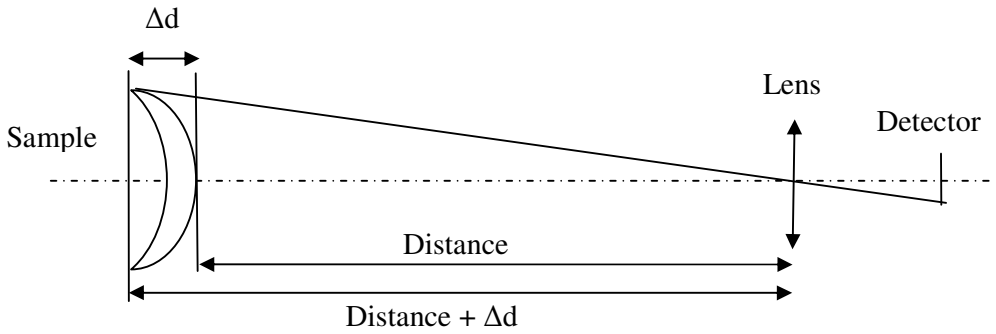

Figure 14 Non uniformity of the distance Sample – Entrance pupil

5.2 Measurement of DOLP and AOP parameters

Measured DOLP profiles were compared to theoretical DOLP. As shown on Figure 15 the measured DOLP are always smaller than expected values while the field is increasing. The DOLP error is up to 0.11 at the edge (11% DOLP). It has a strong impact on the final result as it is related to the local slope of the surface. That error is due to an important amount of flare light in the setup.

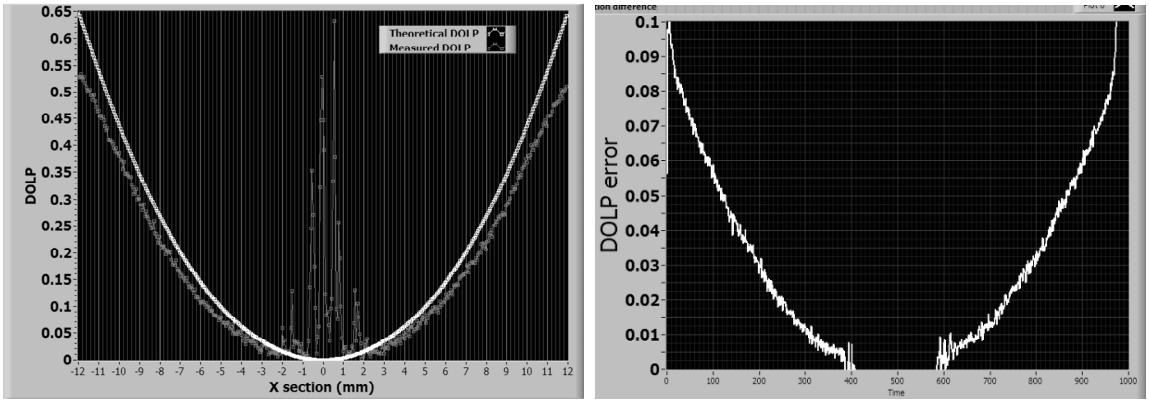

Figure 15: (a) Measured and Theoretical DOLP profiles, 1'' spherical commercial sample, ROC=20.6mm; (b) Deviation

If we call $\mathbf{I_0}$ the intensity of the flare light, $\mathbf{I_S}$ and $\mathbf{I_P}$ respectively the intensity of s-polarized and p-polarized light, $\mathbf{DOLP_{mes}}$ and $\mathbf{DOLP_{th}}$ respectively the measured and the theoretical DOLP, we can see the effect on the DOLP deviation:

$$\Delta_{DOLP} = DOLP_{measured} - DOLP_{theoretical}$$
$$\Delta_{DOLP} = \frac{2I_0}{I_S + I_P + 2I_0} \times DOLP_{th} = K \times DOLP_{theoretical} \quad (4)$$

That leads to a DOLP error proportional to the DOLP expected value. That assumption was verified experimentally. The K constant depends only on the amount of flare light which is related to the experimental setup. Therefore it is possible to measure it and then to correct systematically the DOLP error. That compensation was implemented and gave excellent results. Figure 16 shows corrected DOLP and the new deviation. The error was put down 0.4% pic-to-valley.

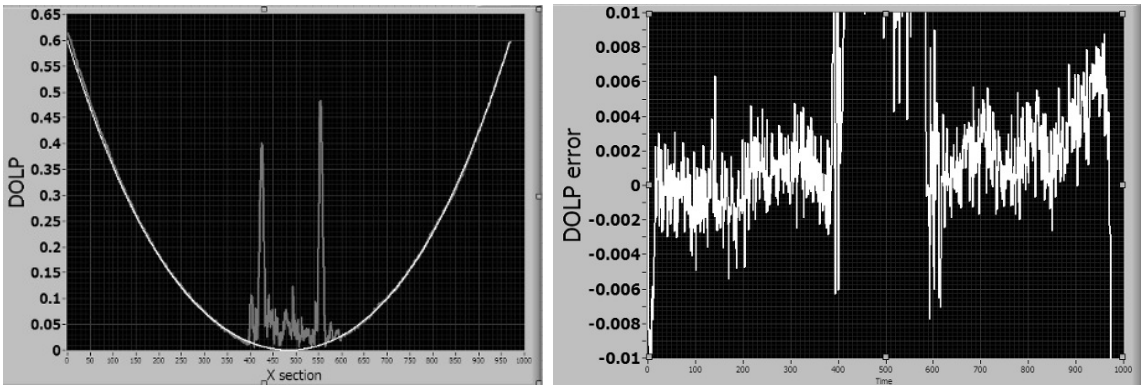

Figure 16 : Calibrated an theoretical DOLP, 1'' spherical commercial sample, ROC=20.6mm; (b) Deviation

Similar results have been observed on commercial spherical and aspheric optics with Radius Of Curvature ranging between 15mm to 105mm. The DOLP correction performed here does not take into account any field dependency. The next step should be to perform a complete calibration of DOLP and AOP values using an angle controlled reflecting plane. Then we could build a calibration matrix for each angle. The real noise appears as a high frequency modulation of the symmetric remaining artifact. Its amplitude is around 100nm.

6. CONCLUSION

The principle of a polarization imaging system for 3D reconstruction of optical elements was successfully demonstrated. A complete setup based on an unpolarized illumination and Bossa Nova Technologies' linear Stokes polarization camera was designed. A dedicated reconstruction algorithm based on the off-the-shelf Frankot-Chellapa algorithm was developed and tested on several commercial samples. The described setup performances were evaluated by comparing measured section profiles and theoretical profiles given by constructors. The samples tested with the method were one and two inches diameters, spherical and aspheric, with Radius of Curvature ranging from 15mm to 110mm and Departure From Sphere ranging from 0 to 800µm. The best accuracy obtained was 25µm with this setup. This is very encouraging as the current setup was based on relatively cheap components and no specific calibrations or signal/image processing was performed.

This work has been sponsored by a SBIR phase I grant from the National Science Foundation.

REFERENCE

[1] Miyazaki, D., Tan, R. T., Hara, K., Ikeuchi, K., 2003. "Polarization-based Inverse Rendering from a Single View". IEEE Int. Conf. on Computer Vision, Nice, France, vol. II, pp. 982-987, (2003).

[2] Miyazaki D., Takashima N., Yoshida A. Hara E. Ikeuchi K. "Polarization-based Shape Estimation of Transparent Objects by Using Raytracing and PLZT Camera", Proceedings of SPIE (Polarization Science and Remote Sensing II, Part of SPIE's International Symposium on Optics and Photonics 2005), Vol. 5888, pp. 1-14, San Diego, CA USA, Aug. 2005, (2005)

[3] Miyazaki, D., "Calculation of surface orientations of transparent objects by little rotation using polarization", Senior Thesis submitted to the Department of Information Science on February 15, 2000

[4] S. Rahmann, “Inferring 3d scene structure from a single polarization image,” in Conference on Polarization and Color Techniques in Industrial Inspection, volume 3826 of SPIE Proceedings, pp. 22–33, June 99.
[5] Rahmann, S., Canterakis, N., 2001. “Reconstruction of Specular Surfaces using Polarization Imaging”. Int. Conf. on Computer Vision and Pattern Recognition, Kauai, USA, vol. I, pp. 149-155, (2001).
[6] S. Rahmann and N. Canterakis, “Reconstruction of specular surfaces using polarization imaging,” in IEEE Computer Vision and Pattern Recognition (CVPR01), volume I, Kauai, USA, pp. 149–155, December 2001.
[7] Atkinson Gary A., Edwin R. Hancock, “Multi-view Surface Reconstruction using Polarization”, Department of Computer Science, University of York, IEEE International Conf. on Computer Vision, (2005)
[8] Atkinson Gary A., Edwin R. Hancock, “Recovery of Surface Orientation From Diffuse Polarization”, Department of Computer Science, University of York, IEEE Transaction on image processing, Vol. 15, n°6, (June 2006)
[9] Atkinson Gary A., “Surface Shape and Reflectance Analysis Using Polarization”, submitted for the degree of Doctor of Philosophy, Department of Computer Science, University of York, May 2007, (2007).
[10] Morel Olivier, Meriaudeau Fabrice, Stolz Christophe, Gorria Patrick, “Polarization Imaging Applied to 3D Reconstruction of Specular Metallic Surfaces”, in Machine Vision Applications in Industrial Inspection XIII; Jeffery R. Price, Fabrice Meriaudeau; eds., Proc. SPIE 5679, 178–186 (San Jose, California, USA, 2005).
[11] Morel Olivier, Meriaudeau Fabrice, Stolz Christophe, Gorria Patrick, “Active Lighting Applied to 3D Reconstruction of Specular Metallic Surfaces by Polarization Imaging”, Thesis Olivier Morel, Le2i UMR CNRS 5158, 12 rue de la Fonderie, 71200 Le Creusot, France, Optical Society of America (2005).
[12] L. B.Wolff and T. E. Boult, “Constraining object features using a polarization reflectance model,” IEEE Trans. Pattern Anal. Machine Intell. 13, 635–657 (1991).
[13] S. Huard, “Polarized optical wave,” in Polarization of Light (Wiley, 1997).
[14] Frankot Robert T., Chellappa Rama, “A Method for Enforcing Integrability in Shape from Shading Algorithms” IEEE Transactions on pattern analysis and machine intelligence, Vol. 10, n°4, July 1988
[15] J.Scott Tyo, Dennis L. Goldstein, David B. Chenault, Joseph A. Shaw, ”Review of passive imaging polarimetry for remote sensing applications”, Applied Optics 5453, Vol. 45, No. 22, (2006)
[16] Lefaudeux N., Lechocinski N., Breugnot S., Clemenceau, P, Bossa Nova Technologies, “Compact and robust linear Stokes polarization camera”, *SPIE conference,* Polarization: Measurement, Analysis, and Remote Sensing VIII, Volume 6972, 2008